# Scanning thermal microscopy and Raman analysis of bulk fused silica exposed to low-energy femtosecond laser pulses

**Y. Bellouard[1,*], E. Barthel[2], A. A. Said[3], M. Dugan[3], P. Bado[3]**

[1] *Mechanical Engineering Department, Eindhoven University of Technology, Eindhoven, the Netherlands*
[2] *CNRS/Saint-Gobain, Surface du Verre et Interfaces, BP 135, F-93303 Aubervilliers, France*
[3] *Translume Inc., 655, Phoenix Drive Ann Arbor, MI, USA*
[*] *Corresponding author: y.bellouard@tue.nl*

**Abstract:** Low energy femtosecond laser pulses locally increase the refractive index and the hydro-fluoric acid etching rate of fused silica. These phenomena form the basis of a direct-write method to fabricate integrated glass devices that are of particular interest for optofluidics and optomechanical applications. Yet the underlying physical mechanism behind these effects remains elusive, especially the role of the laser polarization. Using Scanning Thermal Microscope and Raman spectrometer we observe in laser affected zones, a localized sharp decrease of the thermal conductivity correlated with an increased presence of low-number $SiO_2$ cycles. In addition, we find that a high correlation exists between the amount of structural changes and the decrease of thermal conductivity. Furthermore, sub-wavelength periodic patterns are detected for high peak power exposures. Finally, our findings indicate that, to date, the localized densification induced by femtosecond laser pulses remains well below the theoretical value achievable in mechanically densified silica.



**OCIS codes:** (230.7370) Optical devices: Waveguides, (320.7130) Ultrafast optics: Ultrafast processes in condensed matter, including semiconductors (160.2750) Materials: Glass and other amorphous materials

## References and Links

1. K. M. Davis, K. Miura, N. Sugimoto, and K. Hirao, "Writing waveguides in glass with a femtosecond laser," Opt. Lett. **21**, 1729-1731 (1996).
2. A. Marcinkevičius, S. Juodkazis, M. Watanabe, M. Miwa, S. Matsuo, H. Misawa, and J. Nishii, "Femtosecond Laser-assisted three-dimensional microfabrication in silica," Opt. Lett. **26**, 277-279 (2001).
3. S. Nolte, M. Will, J. Burghoff, and A. Tuennermann, "Femtosecond waveguide writing: a new avenue to three-dimensional integrated optics," Appl. Phys. A: Mater. Sc. Proc. **77,** 109-111 (2003).
4. Y. Bellouard, A. Said, M. Dugan, and P. Bado, "Fabrication of High-Aspect Ratio, Micro-Fluidic Channels and Tunnels using Femtosecond Laser Pulses and Chemical Etching," Opt. Express **12**, 2120-2129 (2004), http://www.opticsinfobase.org/oe/abstract.cfm?URI=oe-12-10-2120.
5. C. Hnatovsky, V. R. Bhardwaj, R. S. Taylor, E. Simova, P. P. Rajeev, D. M. Rayner, and P. B. Corkum, "Fabrication of microchannels in glass using focused femtosecond laser radiation and selective chemical etching," Appl. Phys. A **84**, 47-61 (2006).
6. R. Taylor, C. Hnatovsky, and E. Simova, "Applications of femtosecond laser induced self-organized planar nanocracks inside fused silica glass," Laser Photon. Rev. **2**, 26-46 (2008). doi: 10.1002/lpor.200710031
7. Y. Shimotsuma, P. G. Kazanski, Q. Jiarong, and K. Hirao, "Self-Organized Nanogratings in Glass Irradiated by Ultrashort Light Pulses," Phys. Rev. Lett. **91**, 247405 (2003).
8. Y. Bellouard, T. Colomb, C. Depeursinge, M. Dugan, A. Said, and P. Bado, "Nanoindentation and birefringence measurements on fused silica specimen exposed to low-energy femtosecond pulses," Opt. Express **14**, 8360-8366 (2006), http://www.opticsinfobase.org/abstract.cfm?URI=oe-14-18-8360.
9. J.W. Chan, T. Huser, S. Risbudand, and D. M. Krol, "Structural changes in fused silica after exposure to focused femtosecond laser pulses," Opt. Lett. **26,** 1726-1728 (2001).
10. S. O. Kucheyev and S. G. Demos, "Optical defects produced in fused silica during laser-induced breakdown," Appl. Phys. Lett. **82**, 3230-3232 (2003).
11. D. M. Krol, "Femtosecond laser modification of glass," J. Non-Cryst. Solids **354**, 416-424 (2008).

#101460 - $15.00 USD Received 30 Sep 2008; revised 4 Nov 2008; accepted 4 Nov 2008; published 11 Nov 2008

12. Y. Bellouard, A. Said, and P. Bado, "Integrating optics and micro-mechanics in a single substrate: a step toward monolithic integration in fused silica," Opt. Express **13**, 6635-6644 (2005), http://www.opticsinfobase.org/abstract.cfm?URI=oe-13-17-6635.
13. Y. Bellouard, M. Dugan, A. A. Said, and P. Bado, "Thermal conductivity contrast measurement of Fused Silica exposed to low-energy femtosecond laser pulses," Appl. Phys. Lett. **89**, 161911 (2006).
14. A. Majumbar, "Scanning Thermal Microscopy," Annu. Rev. Mater. Sci. **29**, 505-585 (1999).
15. D.M. Rayner, A. Naumov, and P. B. Corkum, "Ultrashort pulse non-linear optical absorption in transparent media," Opt. Express **13**, 3208-3217 (2005), http://www.opticsinfobase.org/abstract.cfm?URI=oe-13-9-3208.
16. V. Keldysh, "Ionization in the field of a strong electromagnetic wave," Sov. Phys. JETP **20**, 1307–1314 (1965).
17. X. Liu, D. Du, and G. Mourou, "Laser Ablation and Micromachining with Ultrashort Laser Pulses," IEEE J. Quantum Electron. **33**, 1706-1716 (1997).
18. V. R. Bhardwaj, E. Simova, P. P. Rajeev, C. Hnatovsky, R. S. Taylor, D. M. Rayner, and P. B. Corkum, "Optically Produced Arrays of Planar Nanostructures inside Fused Silica," Phys. Rev. Lett. **96**, 057404 (2006).
19. M. Tomozawa, Y. K. Lee, and Y. L. Peng, "Effect of uniaxial stresses on silica glass structure investigated by IR spectroscopy," J. Non-Cryst. Solids **242**, 104-109 (1998).
20. A. Perriot, D. Vandembroucq, E. Barthel, V. Martinez, L. Grosvalet, C. Martinet, and B. Champagnon, "Raman microspectroscopic characterization of amorphous silica plastic behavior," J. Am. Ceram. Soc. **89**, 596-601 (2006).
21. H. Sugiura and T. Yamadaya, "Raman-scattering in silica glass in the permanent densification region," J. Non-Cryst. Solids **144**, 151-158 (1992).
22. N. Kitamura, Y. Toguchi, S. Funo, H. Yamashita, and M. J. Kinoshita, "Refractive-index of densified silica glass," J. Non-Cryst. Solids **159**, 241-245 (1993).
23. P. Oberson, B. Gisin, B. Huttner, and N. Gisin, "Refracted Near-Field Measurements of Refractive Index and Geometry of Silica-on-Silicon Integrated Optical Waveguides," Appl. Opt. **37**, 7268-7272 (1998), http://www.opticsinfobase.org/ao/abstract.cfm?URI=ao-37-31-7268.
24. L. Zheng, J. C. Lambropoulos, and A. W. Schmid, "UV-laser-induced densification of fused silica: a molecular dynamics study," J. Non-Cryst. Solids **347**, 144-152 (2004).
25. A. Agarwal and M. Tomozawa, "Correlation of silica glass properties with the infrared spectra," J. Non-Cryst. Solids **209,** 166-174 (1997).
26. R. S. Taylor, C. Hnatovsky, E. Simova, D. M. Rayner, M. Mehandale, V. R. Bhardwaj, and P. B. Corkum, "Ultra-high resolution index of refraction profiles of femtosecond laser modified silica structures," Opt. Express **11**, 775-781 (2003), http://www.opticsinfobase.org/oe/abstract.cfm?URI=oe-11-7-775.
27. Y. Shimotsuma, K. Hirao, P. G. Kazansky, and J. Qiu, "Three-Dimensional Micro- and Nano-Fabrication in Transparent Materials by Femtosecond Laser," Jpn. J. Appl. Phys. **44**, 4735-4748 (2005).

## 1. Introduction

Femtosecond laser pulses interact in unusual ways with matter. In particular, low energy pulses applied on fused silica can (i) locally increase the material refractive index [1], and (ii) increase its etching rate when exposed to hydrofluoric acid (HF) [2]. Interestingly, the enhanced etching rate is strongly polarization dependent [5]. These phenomena are of particular interest not only for waveguides fabrication [3] but also for optofluidics and optomechanical device manufacturing [4]. They can be used as the basis for a direct-write method to fabricate glass devices with embedded integrated-optics features such as waveguides.

The ultra-short pulses laser-matter interaction induces a cascade of dynamic events at various time-scales that ultimately lead to a permanent modification of the material structure. In this study, we focus our attention on the permanent material changes. To date, two models have been proposed to explain either the increased refractive index or the enhanced etching rate observed after laser exposure. A first model (proposed by R. Taylor *et al.* and thoroughly discussed in [6]) attributes the enhanced etching rate to the presence of oriented cracks that form capillaries, which speed the acid progression inside the glass. In this model, different polarization states lead to different crack orientations. Depending on the orientation of these cracks, the acid penetration is more or less facilitated. R. Taylor *et al.* divide the pulse energy versus duration space in three regimes [6], each corresponding to a distinctive morphology of the laser irradiated region. Regime I corresponds to a laser irradiated morphology showing smooth homogenous modification. Regime I is obtained using low energy, very short pulses. Regime II is associated with moderate pulse energy (typically above 200nJ) and/or longer pulse duration (above 200 fs) which produce what has been labeled by Shimotsuma *et al.* [7]

#101460 - $15.00 USD Received 30 Sep 2008; revised 4 Nov 2008; accepted 4 Nov 2008; published 11 Nov 2008

as nano-grating patterns. Regime III combines self-organized patterns connected to a more disruptive region. This regime is reached with the highest pulse energy.

The model based on nanocracks does not provide a satisfactory reason for the increased etching rate observed at the lowest fluence (corresponding to regime I in ref [6]) where cracks are not found. Furthermore, we note that assuming that such cracks do exist but have yet to be found, the presence of cracks would relax stress in the glass. This is in contradiction with experimental data showing stress concentration in the vicinity of the laser affected one (LAZ) [8]. This is also in contradiction with the increased Young modulus of the laser affected patterns that was reported in [8]. Finally, we note that nanocracks by themselves do not explain the increase of the refractive index observed in the low-fluence regime (as first reported in [1]).

A second model has been proposed that also explains the increase of the refractive index through local material densification [9,10,11,4] Nanoindentation experiments and birefringence experiments [8] have shown that in the low fluence regime (regime I), an increased Young modulus is observed in the laser affected zone surrounded by a localized stress relaxation zone around the LAZ. These observations support the localized densification hypothesis for the low fluence regime. As pointed out by Agrawal *et al*. [4], in mechanically densified bulk fused silica, both increased refractive index and increased etching rate can be correlated [25]. It is therefore reasonable to assume that a similar correlation between increased refractive index and etching rate can also be formulated for laser induced densification.

This localized densification model explains well both phenomena, increased refractive index and increased etching rate, in regime I; but, it does not explain why the increased etching rate depends on the polarization state of the laser beam. In fact, none of the models proposed so far fully explain the effects of low-fluence laser-beam on fused silica.

This low-fluence regime is of utmost importance for applications in integrated optics and optomechanics as this is the regime used for waveguides writing and also for precision micromachining as illustrated for instance in [12].

*This paper is aiming at filling the knowledge gap concerning the low-fluence regime and in particular the effect of the polarization on the structural modification of the fused silica*. Specifically, we report on new characterization results of laser affected zone fine structures produced under different laser light polarization states. We use Scanning Thermal Microscopy (STM) combined with micro-Raman analysis to systematically investigate low-fluence laser affected zones. The combination of the two methods rules out possible artifacts resulting from the specimen preparation process (by probing the matter below the surface) while providing information related to the local thermal conductivity (SThM), and to microstructure (micro-Raman).

## 2. Experimental methods

### *2.1 Specimens, sample preparation and laser exposure*

Fused silica specimens used for these experiments are made of a high purity fused silica substrate characterized by an OH-content in the range of 600-1000ppm. In a first step, single line patterns are written at a depth of 400 microns below the surface by moving the specimen at a constant speed (500 microns/s) under a focused laser beam. A Ti:Sapphire femtosecond laser setup is used to generate 100fs low-energy pulses at a repetition rate of 250 kHz. The focusing optics consists of a 50X objective with a numerical aperture of 0.55.

The beam waist diameter is typically one micron. We test two sets of laser light polarization: transverse (electrical field perpendicular to the laser writing direction) and longitudinal (electrical field collinear to the laser writing direction). For a given polarization, we wrote lines at gradually increasing fluence levels up to 10 J/cm$^2$. To avoid possible coupling effects between patterns, the distance between two consecutive lines is at least 40 μm (i.e. at least 40 to 50 times the width of the laser beam).

#101460 - $15.00 USD Received 30 Sep 2008; revised 4 Nov 2008; accepted 4 Nov 2008; published 11 Nov 2008

After laser exposure, the specimen is cut down the middle using a diamond saw. The cut surfaces are optically polished and cleaned using sequentially isopropanol and acetone. The average roughness (Ra) of the specimen is about 1 nm for a ten-point mean roughness (Rz) of about 8.2 nm measured over a section of 10 x 4 microns.

### *2.2 Characterization of the laser patterns.*

The analysis of femtosecond lasers radiation effects on glass material poses numerous technological challenges due to the size of the LAZ which restricts the number of analytical tools that can be effectively used. A sub-micron resolution is desired.

Using a high-resolution Scanning Thermal Microscope (SThM), we recently discovered that femtosecond laser pulses leave thermal footprints in the material [13]. Similarly, for structural analysis at the micron scale, Raman spectroscopy has been proven to be a very useful tool. Distinct Raman features attributed to modifications created by femtosecond laser pulses were first reported by Chan *et al.* [9].

- Scanning Thermal Microscope

After thorough cleaning in isopropanol and acetone, the cut specimen surface is analyzed using a Scanning Thermal Microscope. This microscope is an AFM (PSIA XE 100) equipped with a cantilever that has a thermal probe and performs an electrical resistance thermometry measurement under dc mode (more details about SThM techniques can be found in [14]). This technique is particularly advantageous for materials with low thermal conductivity such as fused silica. For these materials, probe-current variations can be linearly correlated to thermal conductivity changes [14].

Laser-exposed patterns have waveguiding properties that make them easy to locate directly in the AFM using a proper illumination scheme of the specimen. Once located, a thermal conductivity contrast image is made for various AFM scan sizes. Thermal conductivity contrast images are built from multiple scan sizes (each being typically 4 x 12 μm). For each scan, we use the same resolution (64 data points/micron). The AFM frequency is set to 0.20 Hz to reduce the thermal probe noise level to an acceptable level and to achieve reasonable processing time. For every scan the same force set point (0.75 nN) and the same probe current (0.80mA) are used. These values gave us optimal results in term of thermal conductivity contrast.

- Raman spectroscopy setup

In a subsequent step, the same specimens were analyzed with a confocal Raman spectrometer (25mW, 532 nm Nd:$YVO_4$ frequency doubled laser, grating with 2400 grooves/mm). Profiles across the laser patterns are first carried out to identify the centre of the laser affected zones. The beam is then focused on the centre of each line with a 100x objective and a 50-microns pinhole. The collection time is 500 seconds per spectrum.

### *2.4 Mechanical densification of bulk fused silica (comparison specimen)*

In this study, we use a mechanically densified fused silica for comparison. This specimen is fabricated using the Belt process (4GPa, 425°C for 10min). A density of 2.36 g/cm$^3$ is obtained from flotation. Note that a standard fused silica has a typical density of 2.2 g/cm$^3$.

## 3. Results and discussion

### *3.1 Optical observations*

Figure 1 shows two optical microscope images of the LAZs for both linear polarizations. The pictures are taken in bright field with transmission lighting (i.e. polarization filters are not used). As expected, the laser patterns show waveguiding properties up to a certain fluence threshold, distinct for the two polarizations.

This threshold is 4.5 J/cm$^2$ in the case of longitudinal polarization and 5 J/cm$^2$ in the case of transverse polarization. The visual aspect of the tracks written above these values is also polarization-dependent as can be seen on Fig. 1.

#101460 - $15.00 USD Received 30 Sep 2008; revised 4 Nov 2008; accepted 4 Nov 2008; published 11 Nov 2008

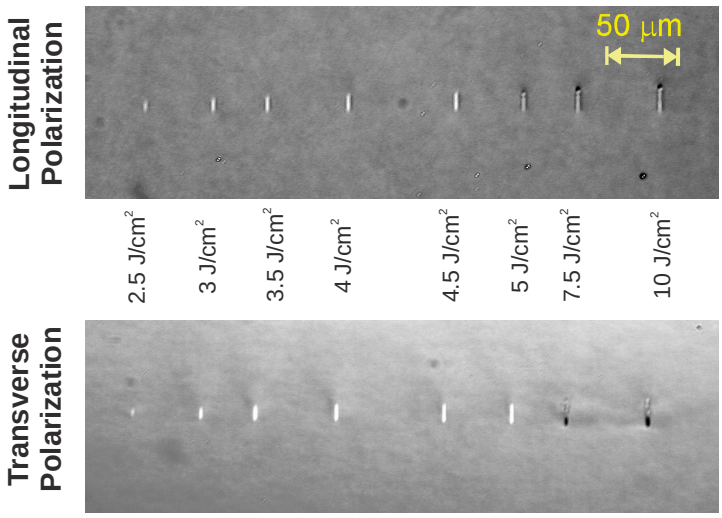


Fig. 1. Optical micrograph of the Laser Affected zones as function of polarization (20 X Bright field image, transmission lighting). LAZs appear as bright spots. Note the lack of wave-guiding properties for the track written in transverse polarization at power higher than 5 J/cm2 and the weak waveguiding properties above 4.5 J/cm2 for the longitudinal polarization.

### *3.2 Scanning Thermal Microscopy imaging*

The laser affected zones are then observed in the SThM operating in dc-mode. A typical SThM image for a LAZ is shown in Fig. 2 (left AFM image). Topographic *and* thermal conductivity maps are acquired at the same time. This pattern corresponds to a fluence of 4 J/cm$^2$ and to a longitudinal polarization state.

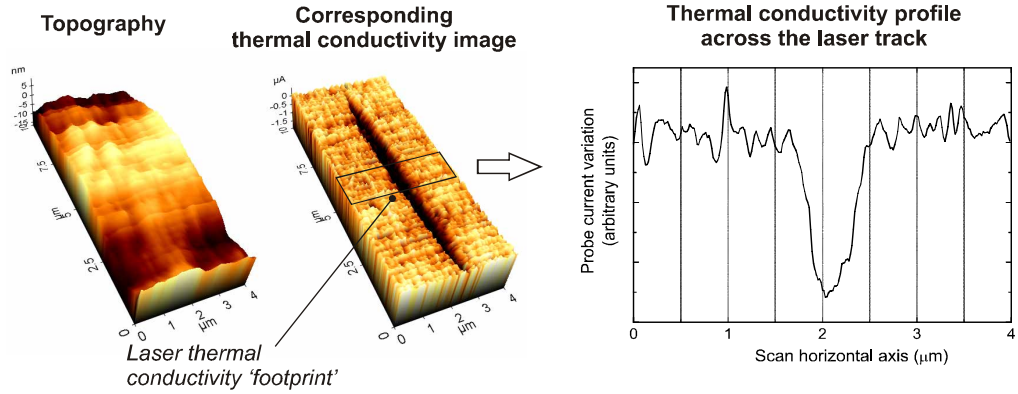


Fig. 2. Typical conductivity data from a laser-affected zone. Topography and probe current variation are acquired simultaneously. Although invisible on the topographic map, the laser-affected zone is clearly identifiable on the thermal conductivity map. The probe current signal indicates a lower thermal conductivity in the laser affected zone.

Although the LAZ is invisible on the topographic information, it is revealed on the probe current variation (thermal conductivity contrast) image. Note that the surface topography has a little effect, if any, on the thermal conductivity image. As discussed in [13], the LAZ geometry matches the zone that shows waveguiding properties. The match between LAZ and SThM is further illustrated in another dramatic example provided in appendix.

Figure 2 shows two important features which are characteristic of SThM maps of low-energy patterns: First, the probe current – and thus the thermal conductivity – is rather homogeneous across the LAZ. Second, a sharp thermal conductivity drop is observed at the

#101460 - $15.00 USD Received 30 Sep 2008; revised 4 Nov 2008; accepted 4 Nov 2008; published 11 Nov 2008

boundary of the LAZ, suggesting the existence of two distinct material phases. The SThM indicates that the thermal drop occurs over a length scale not exceeding 300nm. Considering the SThM resolution (roughly 50nm) and that the measurement is based on thermal diffusion, the transition is most likely to be sharper.

*3.3 Longitudinal polarization*

A compilation of SThM images is shown on Fig. 3 (the contours of the laser affected zone as seen by the SThM have been added to the topographic image).

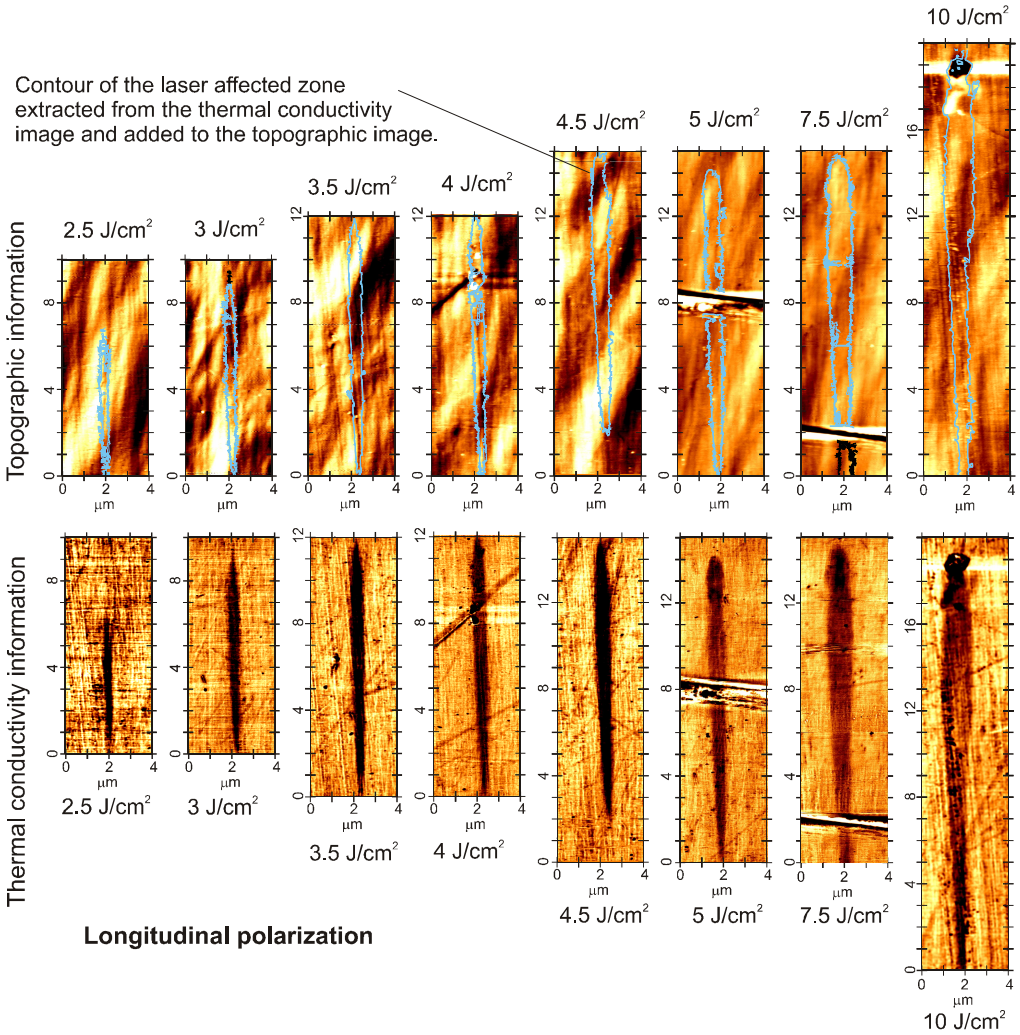


Fig. 3. Set of conductivity map (bottom images) and their corresponding topographic images on a specimen exposed to femtosecond laser light longitudinally polarized and with progressively higher intensity pulses. The contours of the LAZ extracted from the SThM information have been added (light blue contour) on the topology map to emphasize that LAZ do not produce noticeable changes on the specimen topography.

Below 2.5 J/cm$^2$, we do not detect LAZ using either the SThM or a visible microscope. Around 2.5 J/cm$^2$ LAZs become visible. This threshold corresponds to a 50 nJ pulse energy and an instant power of ~ 2.5 $10^{13}$ W/cm$^2$.

As pointed out in [15], this value is in good agreement with the threshold predicted by Keldysh theory of multi-photon ionization in gases and solids [16]. At this energy level, the

#101460 - $15.00 USD Received 30 Sep 2008; revised 4 Nov 2008; accepted 4 Nov 2008; published 11 Nov 2008

affected zone is substantially smaller than the laser spot itself. The affected zone resembles an elongated ellipse. As the pulse energy is gradually increased, both elliptical axes grow. We notice that the pattern departs from an elliptical shape at higher energies (typically above 4.5 J/cm$^2$). As can be seen from the topographic information, the LAZ appearing in the SThM has no direct correlation with topographical features, unlike features like scratches, dirt or cracks that are visible on both images.

*3.4 Transverse polarization*

Similar patterns are found for transverse polarization and illustrated in Fig. 4. Below a certain energy threshold, neither the SThM, nor the optical microscope shows any material modification. The energy threshold at which a pattern is first observed is comparable to that observed in the longitudinal polarization case. Further, the pattern shapes and sizes are comparable up to 4.5 J/cm$^2$. However above this value, we observe the formation of a self-organized pattern in the laser affected zone. These patterns are similar to those observed by Shimotsuma *et al.* [7] and other authors [18] using backscattered electron images in a SEM or a post-etching process. Data obtained above 4.5 J/cm$^2$ are particularly interesting and are analyzed in more details in a sub-paragraph. Figure 5 shows a selection of images taken for various pulse energies gradually increased from 2.5 J/cm$^2$ to 10 J/cm$^2$.

As for the longitudinal polarization, the LAZ revealed by the SThM has no direct correlation with topographical features which emphasize potential material properties changes induced by the laser exposure.

From the observations of LAZs under different polarization conditions, we conclude that there is no evidence of heat accumulation, nor evidences of thermal effect away from the LAZ for the repetition rate considered. In addition, no filamentation is observed at least up to pulse energy levels of 4.5 J/cm$^2$.

Above 4.5 J/cm$^2$, we are in a different regime where we observe sub-wavelength self-organizing patterns for the transverse polarization. Note that these self-organizing sub-wavelength patterns may be present in the longitudinal polarization but simply not visible due to the plane of observation cut. This explanation would be consistent with other sub-wavelength patterns results reported in the literature [7,18].

From the systematic analysis of the laser tracks written at increasing fluence level, we first conclude that:

- Thermal conductivity changes are not found at energy below a threshold fluence of 1.90 J/cm$^2$ which emphasize the non-linear nature of the femtosecond laser-matter interaction.

- Self-organized patterns similar to the one reported by Shimotsuma *et al.* [7] consisting in multiple parallel lines with spatial frequencies typically in the range of 100nm are found when the polarization is transverse and for fluences above 5 J/cm$^2$. Below this threshold value, we found, for both polarizations, a homogeneous SThM pattern comparable to the one shown in Fig. 1.

For each SThM map, we extract an average probe-current drop value. These data are calculated by averaging the probe-current value over a one-micron window in the vertical direction and by calculating the average value over the left and right sides of the laser affected zone. The results for both transverse and longitudinal polarization are shown in Fig. 5. A steep variation of thermal conductivity is observed up to fluences of 3 J/cm$^2$. Above the signal tends to settle around a plateau value. Several measurements have been made with two different probes: one starting from the lower to the higher power and the second one going in the opposite direction (from the highest to the lowest).

#101460 - $15.00 USD Received 30 Sep 2008; revised 4 Nov 2008; accepted 4 Nov 2008; published 11 Nov 2008

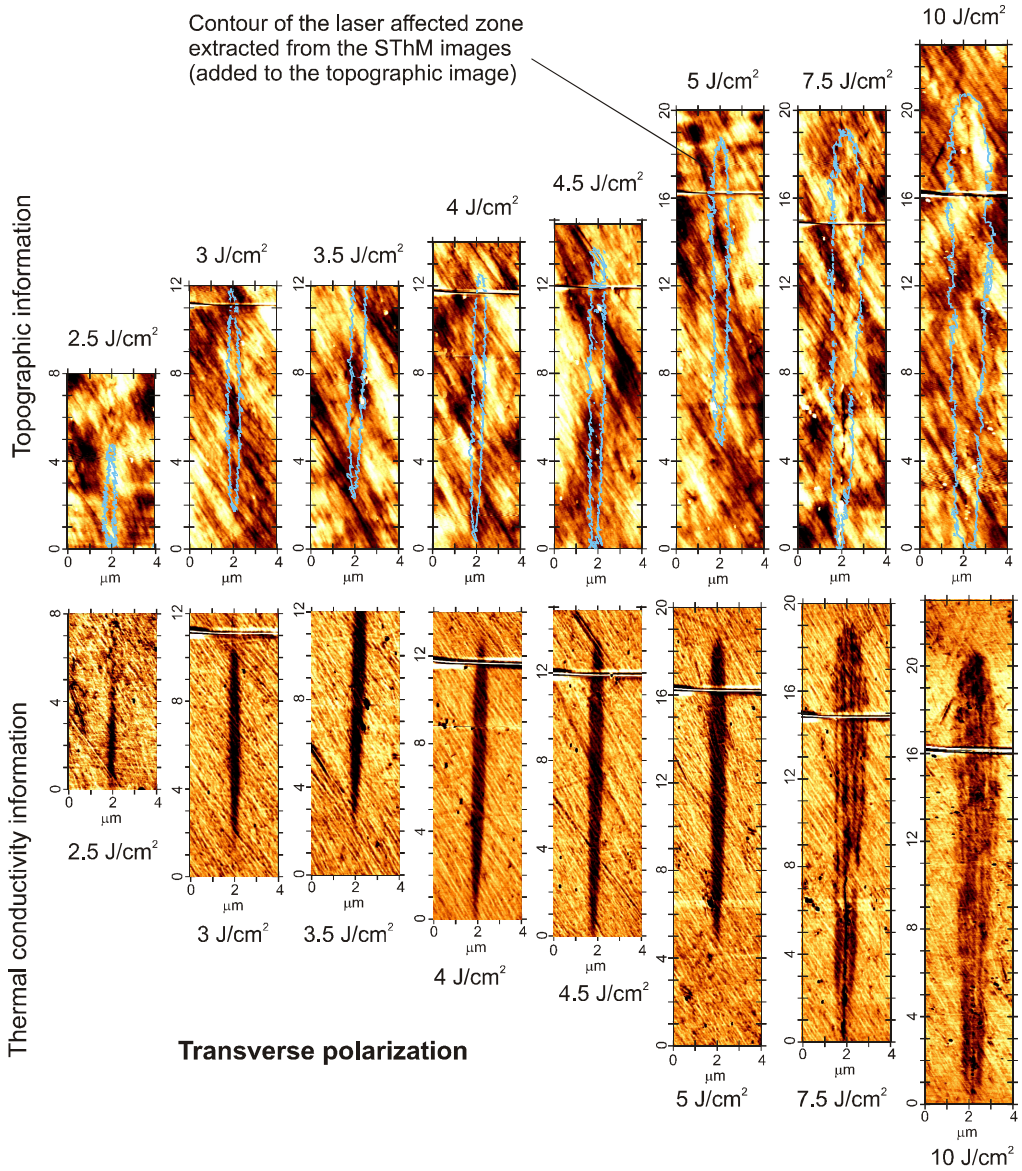


Fig. 4. Selection of SThM and simultaneous topographic images of patterns exposed to pulses with transverse polarization. The horizontal black zones spanning across some of the scan corresponds to a surface scratch (all but 2.5 and 3.5 J/cm$^2$) as revealed by the topographical map. The contours of the LAZ extracted from the SThM information have been added (light blue contour) on the topology map to emphasize that LAZ do not produce noticeable changes on the specimen topography.

For the transverse polarization, the probe current variation is difficult to define above 7.5 J/cm$^2$ due to the presence of the so-called nano-gratings. The multiple points shown for these fluence levels correspond to individual line of the "nanogratings".

From these data, we note that:

- For both polarizations, the thermal conductivity first rapidly decreases as the fluence increases until it reaches a plateau where the thermal conductivity remains constant. In absolute values, these decreases of thermal conductivity seem to be gradually reduced above 5 J/cm$^2$ for the transverse polarization.

#101460 - $15.00 USD Received 30 Sep 2008; revised 4 Nov 2008; accepted 4 Nov 2008; published 11 Nov 2008

However, we caution this observation since the fine-structures found in the nano-gratings are close to the resolution of the SThM. Therefore, the decrease of thermal conductivity might be underestimated.

- A slightly higher decrease of thermal conductivity in the case of transverse polarization is observed (at least up to fluence level of 5 J/cm$^2$).

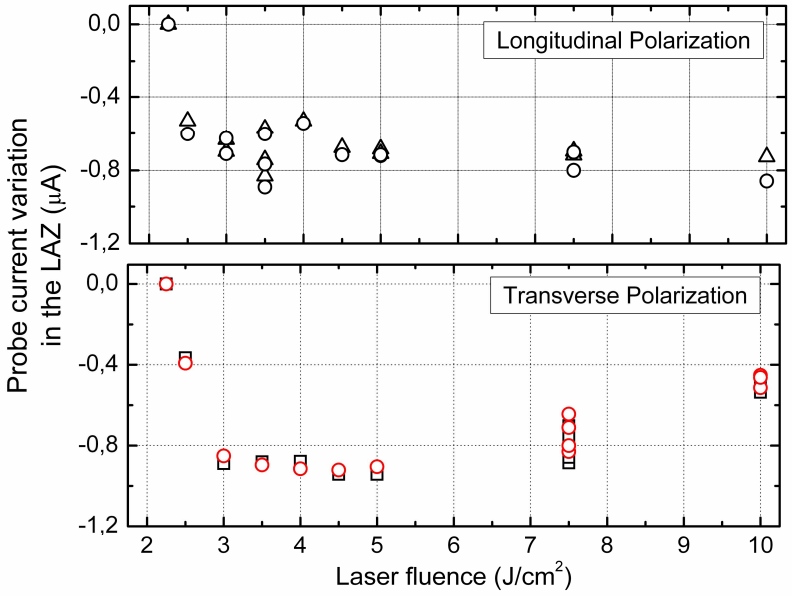


Fig. 5. Relative variation of SThM probe currents as a function of fluence, for two different polarizations: longitudinal (top graph) and transverse (bottom graph).

*3.5 SThM analysis of sub-wavelength patterns*

The LAZ created with the highest energy pulses and transverse polarization show clearly distinct, self-organized patterns with sub-wavelength dimensions. These patterns are similar to those detected by others [7,18]. Figure 6 shows the thermal conductivity image and the corresponding topographical information of the LAZ corresponding to 7.5 J/cm$^2$.

For this particular example, we notice the presence of a crack aligned along the LAZ and located precisely in the middle. Note that unlike LAZs that appear only on thermal conductivity images, cracks and other topographic features like surface scratches appear on *both* – thermal conductivity and topographic images. The SThM coupled with the topographical information allows a precise localization of the crack (it appears as a sharp and intense drop on the probe current signal and as a clear distinct feature on the topography map). We interpret this crack as a direct consequence of the laser exposure considering its particular location and orientation. (Another illustration of crack seen with a SThM is provided in the Appendix.)

#101460 - $15.00 USD Received 30 Sep 2008; revised 4 Nov 2008; accepted 4 Nov 2008; published 11 Nov 2008

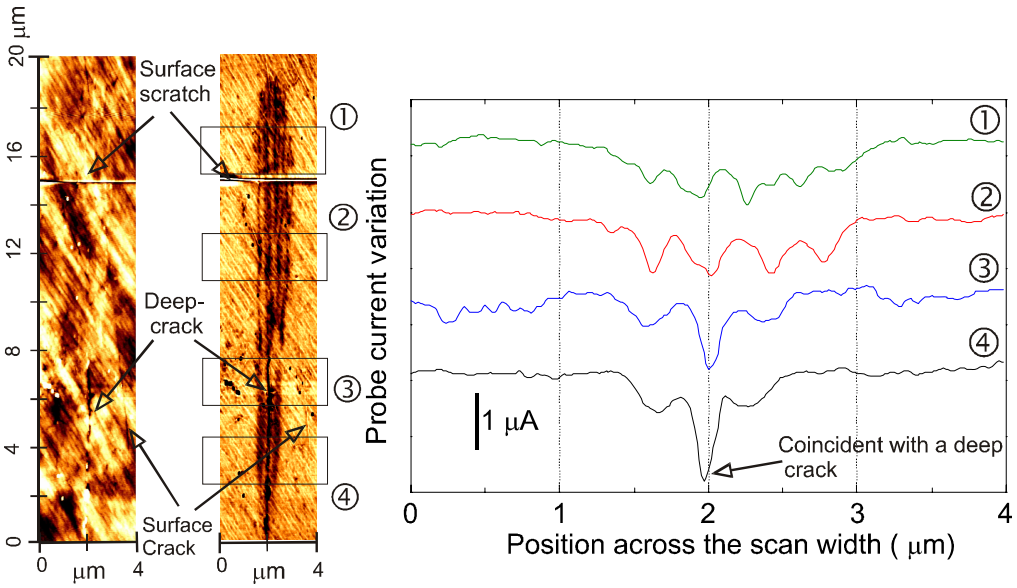


Fig. 6. SThM analysis of a high energy pattern (7.5 J/cm$^2$) obtained with a transverse polarization. Left: topography and corresponding scanning contrast measurement. Oblique regular striation results from polishing. Right: probe current variation across the scan width. Each profile is averaged over a window spanning across 2 um in the vertical direction.

This observation indicates that cracks found in nano-gratings – if present – do not form during the laser exposure *per se* but rather due to a change of material structure resulting from the laser exposure. We will further develop this point in the discussion section. SThM yields intriguing information related the LAZ that we attribute to changes in the material intimate structure. To support this hypothesis, we conducted a systematic Raman spectroscopy analysis of the same laser affected patterns. This approach offers the advantage to be non-invasive and to provide structural information about the material lattice, in particular below its surface. Previous Raman spectra investigations of femtosecond laser patterns were reported before (for instance [9]) but not combined with a SThM study. Furthermore, the effect of the polarization on Raman spectra has not been reported.

*3.6 Micro-Raman analysis*

Raman spectra of a laser affected zone (longitudinal polarization, 5 J/cm$^2$) and of a pristine zone of the same specimen are compared in Fig. 7 (right). For reference, in the Fig. 7 (left) we show the spectrum of mechanically-densified bulk-silica and that of a pristine bulk-silica. Features that are characteristic of a densified material are found on both the laser affected and the mechanically densified sets of curves: The main band at 400 cm$^{-1}$, the D1 and D2 peaks at 490 and 605 cm$^{-1}$ (related to the vibrations of 4 and 3-membered rings respectively), shift to higher wavenumbers and the main band becomes narrower [19].

In the case of femtosecond laser exposed specimens, the D2 peak significantly increases in intensity, an effect which is also observed for the mechanically densified sample [20]. The D2 peak is not only the signature of rare 3-tetrahedra cycles but also signals more general structural modifications. It has been demonstrated that the D2-peak shift is sensitive to the density [21]. Unlike the D1-peak shift, the D2-peak shift is relatively easy to measure since its peak does not overlap with the main band.

To simultaneously quantify the D1 and D2 features, the contribution of the main band was subtracted by interpolation of a cubic splines baseline over the 400-1000 cm$^{-1}$ range through the D1 and D2 regions. With this procedure, not only the integrated areas of the D1 and the D2 peaks can be calculated but also the 800 cm$^{-1}$ band, which is later used for normalization. The main source of error with this method is the distortion of the baseline due to the shift of

#101460 - $15.00 USD Received 30 Sep 2008; revised 4 Nov 2008; accepted 4 Nov 2008; published 11 Nov 2008

the main band. Fitting the D2 line with a Lorentzian profile after baseline subtraction, we calculate a shift from 601 $cm^{-1}$ (pristine) to 608 $cm^{-1}$ (densified).

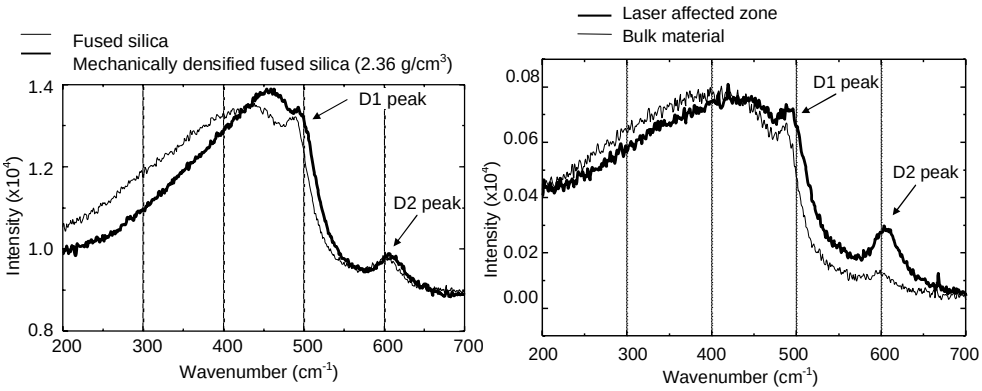


Fig. 7. Raman spectra of raw silica and a mechanically densified fused silica (left) and Raman spectra of the laser affected zone compared to a Raman spectra in pristine zone of the material (Right).

From literature data [21], this noticeable shift suggests a densification of approximately 8%, a value which is supported by the shift of the main band. Assuming this level of densification and using Kitamura *et al.* work on shock densified silica [22], we extrapolate a local increase of refractive index of about $3.10^{-2}$. This result is an order of magnitude larger than the reported increase of refracted index in fused silica expose to femtosecond laser pulses (typically $5.10^{-3}$).

To explain this discrepancy, we formulate two hypotheses. One possibility is that the refractive index measurement reported so far are averaged values of the laser affected zone and its immediate surrounding. This explanation is plausible considering the small size of the LAZ and the limited spatial resolution of local refractive index measurement technique [23].

A second possibility is that the structure of "laser densified" fused silica is different from the structure of shock-densified silica, therefore preventing the use of shock densified silica data to calculate femtosecond-generated, refractive index change.

Raman spectra were recorded for different fluences. The integrated intensities of the D1 and D2 peaks normalized by the intensity of the 800 $cm^{-1}$ band are shown in Fig. 8. A typical error bar is ±0.15 after baseline subtraction over the 400-1000 $cm^{-1}$ range. Note that the noise level is somewhat lower if a more localized baseline fit is used as evidenced by Fig. 9.

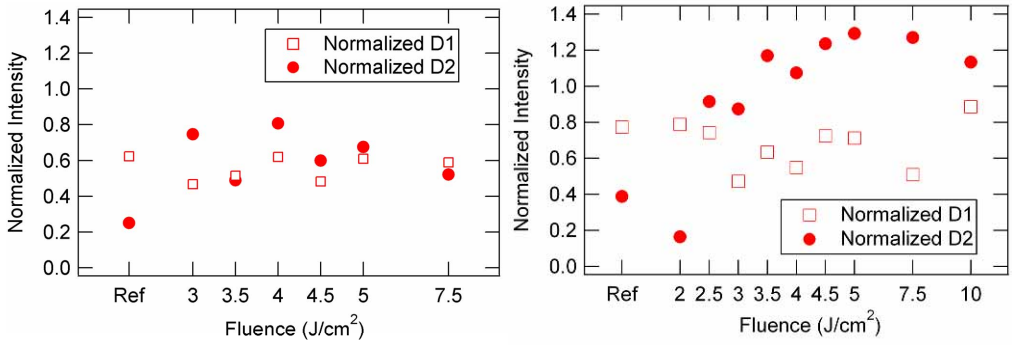


Fig. 8. Raman spectra for transverse (left) and longitudinal polarization (right): intensity variation of peaks D1 and D2 normalized to the 800 $cm^{-1}$ band intensity as a function of laser fluence. "Ref" is a reference measurement made in pristine zones (i.e. not exposed to the laser beam) of the specimens.

#101460 - $15.00 USD Received 30 Sep 2008; revised 4 Nov 2008; accepted 4 Nov 2008; published 11 Nov 2008

Surprisingly, we find that the intensity of the de-convoluted D1-peak is unaffected by laser irradiation. It is usually reported that the D1 intensity increases with density but, in these cases, the bare amplitude of the D1 peak is often reported without deconvolution of the main band. Note that molecular dynamics simulations [24] usually predict an increased number of 4-membered rings. It should be noted [24] that even in very low-quantities (typically a few %) 3-tetrahedra cycles lead to a distinctive signature in the Raman data.

For both polarizations, a plateau is found. For the longitudinal polarization, a gradual increase of the D2 peak intensity is observed, which flattens out rapidly with the increasing fluence levels. This result indicates that above a given value and at least up to 5 J/cm$^2$, increasing the fluence level does not lead to further increase of the number of 4-members rings. Another important observation is that even above 5 J/cm$^2$ where nano-gratings are found, there are still evidences of structural changes in the material that can be related to densification phenomena.

The D2-peak information shows that the material structure is strongly polarization dependent and this, even at fluences level where nano-gratings are observed. To illustrate this observation, Raman spectra for two representative fluences levels for the two polarizations are shown in Fig. 9. This result is quite remarkable. For a transverse polarization, the D1 and D2 peak intensities are similar. For a longitudinal polarization, the D2 peak intensity is significantly and consistently larger. 3-tetrahedra cycles are therefore more numerous in the longitudinal polarization cases.

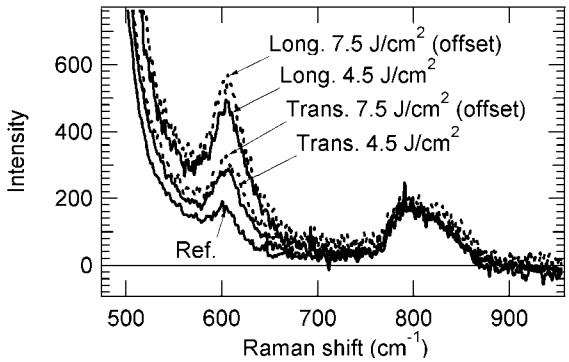


Fig. 9. The D2 peak and the 800 cm$^{-1}$ band in Raman spectra measured for two different polarizations and two characteristic fluence levels. For clarity the 7.5 J/cm2 spectra were offset vertically by 25 intensity units to avoid superposition with the 4.5 J/cm$^2$ spectra. The near perfect superposition of the peaks for transverse polarization on the one hand and longitudinal polarization on the other hand illustrate the typical reproducibility of the Raman characterization. "Ref" is a reference measurement made in a pristine zone (unexposed to the laser beam) of the same specimen.

## 4. Summary of the observations

We have shown that for low-energy femtosecond pulses with transverses and longitudinal polarizations:

- Laser affected zones are observable above fluence levels in the range of 2 J/cm$^2$. Below this threshold value, no visible patterns are found.
- Above approximately 5 J/cm$^2$, a second regime is found where laser generated lines no longer exhibit waveguiding properties.
- Our SThM data show that at low-energy pulses, femtosecond laser irradiation induces a localized decrease of thermal conductivity on fused silica for both polarizations. At this point, we attribute the decrease of thermal conductivity to the increase number of phonons scattering events taking place in the LAZ possibly due to an increased number of shorter rings and/or defects.
- Raman data confirm a localized increase of material density for both polarizations and this even at higher fluence levels where nano-gratings are

#101460 - $15.00 USD Received 30 Sep 2008; revised 4 Nov 2008; accepted 4 Nov 2008; published 11 Nov 2008

observed. A localized increase of material density is consistent with an increase of refractive index as it is observed for fused silica exposed to low-energy pulses. Here we are able to provide a first estimation of the increase of density. Based on the D2-peak shift, we estimate this femtosecond driven densification to be about 8%. This is appreciably less than the densification obtained with other processes, such as mechanical densification. Obtaining higher densification and higher index of refraction with femtosecond lasers would have significant commercial implications. .

- Raman data together with the SThM maps further supports the existence of two material phases. In addition, a sharp gradient is observed between the two phases.
- Upon increasing the fluence level, a consistent behavior is found for both polarizations and for both investigation tools: the signal rapidly saturates and a plateau is found. Although further work is needed to establish the relation between thermal conductivity and densification level, qualitatively, a direct correlation is found between the two parameters. Another important and practical consequence is that above a threshold fluence value (up to at least 5 J/cm$^2$) no additional increase of density is observed. Note this is consistent with previous observations [4] where an optimal laser power was found to boost etching.

## 5. Discussion and conclusion

We note significant differences between the two polarization states: the decrease of thermal conductivity is more pronounced for the transverse polarization than for the longitudinal polarization. On the opposite, Raman measurements indicate higher number of 3-cycles in the case of longitudinal polarization.

It has been shown that specimens exposed to longitudinally polarized pulses are etched at a slower rate. 3-cycles $SiO_2$ ring have smaller Si-O-Si bond angles, which can be correlated to a faster etching rate than higher cycles numbers [25]. Therefore, one would expect the longitudinal polarization to etch faster, which is opposite to what is observed.

A possible explanation to this observation is that a more complex substructure may be present: rather than being introduced homogeneously within the laser affected volume, lamellas containing a higher number of 3-order rings would form in a structured manner and according a direction set by the laser polarization (perpendicular to the track for longitudinal polarization and parallel to the line for transverse polarization). Due to the high-number of 3-order rings, these lamellas would be etched faster than the rest. Longitudinally aligned lamellas would favor a rapid penetration of the HF toward the laser line while transversely aligned would on the contrary slow it down (according a mechanism somewhat similar to the one proposed by R. Taylor *et al.* [6] for oriented cracks to explain the increase etching rate). Note that the model proposed by Shimotsuma *et al.* [27] to interpret nano-grating formations potentially supports the existence of self-organized structures with lower periodicity than 100nm. At this point, we acknowledge that our interpretation based on the presence of nano-scale size organized-patterns to explain the polarization dependence of etching rates at low-fluences is speculative, as we are lacking sufficiently detailed data to support it.

Nevertheless an important conclusion of this study is that both SThM and Raman experiments show that the two polarizations lead to different material structures that have different susceptibility to HF etching. Based on these combined observations we propose a refined model of the material modification resulting from low fluence femtosecond laser exposure. Above a threshold fluence (found at 1.90 J/cm$^2$ for our experimental setup), the material is locally densified. An estimate of this densification level is 8%. We have been unable to obtain higher densification to date. Consequent to the densification, the material surrounding the LAZ is put under tensile stress. Note that this is a necessary condition to accommodate the localized change of volume resulting from the densification. This tensile stress is mainly responsible for birefringent observations. (The presence of tensile stress was confirmed by measurement of birefringence using digital holography [8].)

#101460 - $15.00 USD Received 30 Sep 2008; revised 4 Nov 2008; accepted 4 Nov 2008; published 11 Nov 2008

The shape of the densified zones is elliptic. The stress concentration is the highest at the tip of the elongated axis of the laser affected zone. The higher the ellipse length over width ratio, the more elevated the stress concentration level at the tip. Our Raman observations suggest that self-organized patterns observed at higher fluence are also composed of densified zones (note that the scanning electron microscope back-scattering images of similar patterns obtained by Shimotsuma *et al.* [7, 27] also supports this hypothesis). In this structure, the stress gradient will be particularly high. It is therefore not surprising to find cracks preferably forming in these patterns. One may expect that above some threshold stress level a crack would nucleate precisely at location where stress concentrations are the highest, starting from the tip of the elongated densified zone and propagating along its long axis.

Another important conclusion from these observations is that the self-organized patterns are unlikely to be "nano-cracks" (at least for the fluence regime studied) but rather regions where the material structure has been modified in a similar manner than at lower pulse energies, i.e. the nano-grating are formed of densified zones. To support this conclusion we note that when cracks are present, they appear very distinctly on both topographic and thermal conductivity map. Therefore when we do not observed cracks we conclude they are in fact not present (for instance the pattern obtained for pulse energy of 10 J/cm$^2$ shows no crack although it is obtained at significantly higher energy that the pattern shown in Fig. 6). However, because of high stress concentration consistent with a localized density increase, cracks may be eventually initiated in certain spot of the self-organized patterns, as is clearly visible in Fig. 6. For this particular case, it is not possible to conclude whether this crack was formed soon after laser exposure or much later when the specimen was cut to be examined by the SThM. At even higher fluence levels (not studied here), the likelihood of finding cracks may be significantly higher as the number of parallel densified patterns gradually increases, further loading the material up to its rupture point. This could for instance be the case for regime III. Another possibility to explain the different morphology of regime III is the formation of other defects like oxygen deficiency centers [ODC (II)] as suggested in [10] that would further weaken the material structure.

## Appendix

The composite figure below shows different observations of a given LAZ using two microscopes.

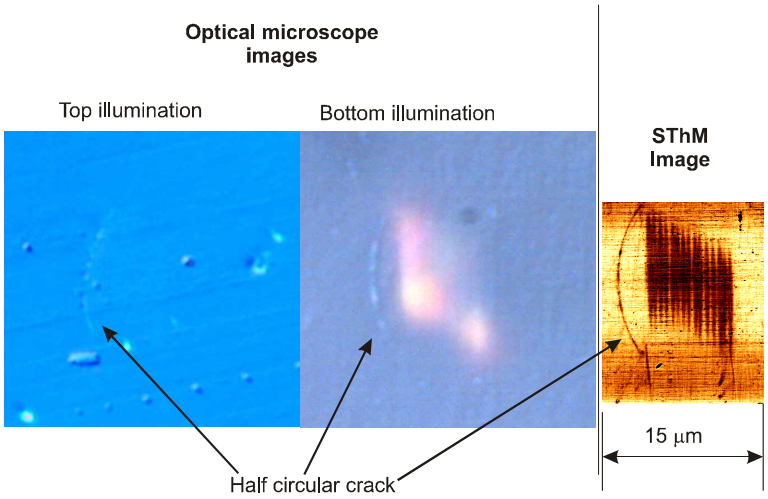


Fig. 10. Illustration of laser affected zones observed with different microscope. LAZ patterns were written with a longitudinal polarization and a fluence of 2.5-3 J/cm$^2$ under the same exposure conditions described in this paper.

#101460 - $15.00 USD Received 30 Sep 2008; revised 4 Nov 2008; accepted 4 Nov 2008; published 11 Nov 2008

It illustrates the STHM capability to provide excellent information on Laser Affected Zones. The laser affected pattern is made by writing fifteen adjacent lines next to another to form a wide laser affected zone. The left image was collected with an optical microscope (100X objective with above sample illumination). Oblique striations resulting from the polishing are visible. The center image shows the exact same location, this time observed in transmitted illumination mode. The Laser affected zones have waveguiding properties as can be seen from this image: some of the illumination light transmitted through the specimen is locally guided and shows up as a well-defined pattern. The image on the rights, show again the same location, this time observed with the SThM microscope. The fine structure of the LAZ, which went undetected on the left photograph, is clearly revealed with the SThM. Note the half-circular cracks visible on the three images. Cracks also appear on SThM image since they locally modify locally the heat conduction properties. However, contrary to LAZ, the profile of a crack is sharper (See Fig. 11). Further, cracks are also visible on the topology image acquired by the AFM at the same time than the SThM one. The cross-correlation of the two images allows us to discriminate clearly cracks from localized structural modification of the heat conduction properties as emphasized earlier in this paper. The half circular crack can most likely be correlated to the presence the laser affected zone and may result from the building up of stress resulting from the stacking of multiple adjacent laser affected zones.

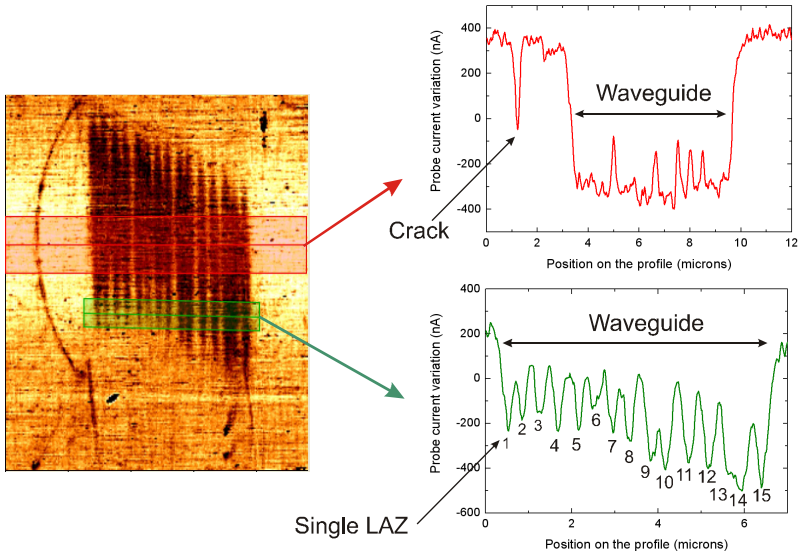


Fig. 11. Averaged thermal conductivity profiles across various regions on the laser affected zone consisting of 15 adjacent single laser patterns. Note the sharp drop resulting from the presence of the half-circular crack (top profile).

These images demonstrate the usefulness of SThM observations to analyze Laser-affected patterns not only spatially but also in term of thermal conductivity properties.

**Acknowledgments**

The authors are thankful to A. San Miguel, S. Le Floch (LPMCN, Lyon) and A. Perriot (SVI, Aubervilliers) for providing the mechanically densified silica sample.

#101460 - $15.00 USD Received 30 Sep 2008; revised 4 Nov 2008; accepted 4 Nov 2008; published 11 Nov 2008